Dynamics of the S(^{1}D) + H_2 Insertion Reaction: A Combined Quantum Mechanical and Quasiclassical Trajectory Study

L. Bañares* and F. J. Aoiz

Departamento de Química Física Facultad de Química, Universidad Complutense 28040 Madrid, Spain

P. Honvault and J.-M. Launay

PALMS, UMR 6627 du CNRS, Université de Rennes 1, Campus de Beaulieu, 35042 Rennes Cedex, France

Received: October 14, 2003; In Final Form: January 8, 2004

Accurate three-dimensional quantum mechanical (QM) scattering calculations of integral and differential cross sections for the S(^{1}D) + H_2 ($v = 0$, $j = 0$, 1) insertion reaction have been carried out at a collision energy of 2.24 kcal/mol. Additionally, quasiclassical trajectory (QCT) calculations have been performed for the same reaction at 2.24 and 3.96 kcal/mol collision energies. The assignment of product quantum states in the QCT method has been carried out using a Gaussian-weighted binning procedure, which has proved to be more accurate than the usual histogramatic method. QM and QCT reaction probabilities at total angular momentum $J = 0$ as a function of collision energy within the range 0−11.5 kcal/mol for the S(^{1}D) + H_2 ($v = 0$, $j = 0$) reaction are also reported. The theoretical results have been used to simulate the available experimental data in the form of differential cross sections and product translational energy distributions. A general good agreement is found between theory and experiment for this prototypic insertion reaction.

I. Introduction

After the success of quantum reactive scattering theory in reproducing the most fundamental features of the dynamics of the simplest abstraction reactions measured in high-resolution molecular-beam experiments (see refs 1−3 for recent reviews), the interest is now moving toward the understanding of the dynamics of another class of chemical reactions: those that are characterized by an *insertion* mechanism.

The reaction between sulfur atoms in their ^{1}D electronically excited state and hydrogen molecules belongs to that class of *insertion* reactions, of which the O(^{1}D) + H_2 reactive system has been the most studied experimentally and theoretically up to date (see, for instance, refs 4−8 for recent works). Other examples of recently studied reactions dominated by an insertion mechanism include the N(^{2}D) + H_2[9,10] and C(^{1}D) + H_2[11,12] systems. The S(^{1}D) + H_2 reaction has in common with O(^{1}D) + H_2 the existence of a deep well corresponding to the $1^1A'$ electronic state of the H_2S stable species. However, in contrast with the O(^{1}D) + H_2 system, this reaction is only slightly exothermic (6.90 kcal/mol) and the well that characterizes the H_2S radical is not as deep (96 kcal/mol) as that for H_2O (168.2 kcal/mol). In addition, the contribution to the dynamics of the *abstraction* reaction over the first $1^1A''$ electronically excited potential-energy surface (PES) at moderate collision energies, which is quite relevant for the O(^{1}D) + H_2 reaction,[5] is negligible here. The collinear barrier of the $1^1A''$ PES for the H_2S is 10 kcal/mol,[13] whereas it is only 2.3 kcal/mol for the H_2O system. These differences in PES topology make of this system an interesting candidate to deepen our understanding of the dynamics of insertion reactions.

The S(^{1}D) + H_2 reaction and its isotopic variants have been studied recently both theoretically and experimentally. In a series of publications, Lee and Liu reported angular distributions and product translational energy distributions for the S(^{1}D) + H_2[14] and S(^{1}D) + D_2[15] reactions at several collision energies using the Doppler-selected time-of-flight technique in combination with crossed molecular beam experiments. In addition, excitation functions for the S(^{1}D) + H_2, D_2, and HD reactions were determined over a wide range of collision energies.[16] From the theoretical side, Zyubin et al.[13] carried out extensive ab initio calculations for the H_2S system at the multireference configuration interaction (MRCI) level of theory with multiconfiguration self-consistent field (MCSCF) reference wave functions for the 1A′, 2A′, 3A′, 1A″, and 2A″ singlet PESs that correlate to S(^{1}D) + H_2. The ground state 1A′ PES was fitted to an analytical function based on the reproducing kernel Hilbert space (RKHS) approach and a Carter−Murrell-type expansion, and the dynamics of the S(^{1}D) + H_2 and D_2 reactions on this PES was studied by means of quasiclassical trajectory (QCT) calculations. Chao and Skodje[17] carried out an extensive QCT study using this PES. Integral and differential cross sections were calculated for all isotopic variants of the reaction and for different rotational quantum states of the diatomic reagents to simulate the experimental results of Lee and Liu in the form of differential cross sections and total and angle-resolved product translational energy distributions. A good general agreement between theory and experiment was found, although significant differences in the more finely resolved quantities were present. Subsequently, an improved ground state 1A′ PES based on the same ab initio data set and using the RKHS interpolation method was produced by Ho et al.,[18] and new QCT calculations performed on this last PES showed that the main results were similar to those obtained on the previous version of the PES.

* Author to whom correspondence may be addressed. Email: banares@legendre.quim.ucm.es.

10.1021/jp037109o CCC: $27.50
Published on Web 02/05/2004

In a recent letter, the first accurate quantum mechanical (QM) scattering calculations for the title reaction at 2.24 kcal/mol collision energy carried out on the PES by Ho et al. were presented.[19] In the present work, we present a full account of the QM calculations of ref 19 in combination with new quasiclassical trajectory (QCT) calculations on the ab initio PES produced by Ho et al.[18] Integral and differential cross sections have been calculated at 2.24 and 3.96 kcal/mol collision energies and for initial H_2 rotational quantum numbers $j = 0$ and 1, which correspond to the conditions of the molecular beam experiments performed by Lee and Liu.[14] In addition, QM and QCT total and vibrational state-resolved reaction probabilities at total angular momentum $J = 0$ for the S(^{1}D) + H_2 ($v = 0$, $j = 0$) reaction have been obtained in the 0−11.5 kcal/mol collision energy range and compared to each other.

II. Theoretical Methods

All the theoretical calculations have been carried out on the $1^1A'$ H_2S ab initio PES of Ho et al.[18]

For the QM scattering calculations, a time-independent method, which employs body-frame democratic hyperspherical coordinates, is employed.[19−23] This method has proved to be very successful in the description of the O(^{1}D) + H_2[24] and N(^{2}D) + H_2[25] insertion reactions. At each hyper-radius ρ, we determine a set of eigenfunctions of a fixed hyper-radius reference Hamiltonian $H_0 = V + T$, which incorporates the total energy with the kinetic energy T arising from deformation and rotation around the axis of least inertia and the potential energy V. At small ρ, the adiabatic states in each sector span a large fraction of configuration space and allow for atom exchange. These states are expanded on a basis of pseudo-hyperspherical harmonics with a maximum grand angular momentum of 348. We retain between 1600 and 7500 functions, depending on ρ (from 1.8 to 15.1a_0). For total angular momentum $J = 0$, the scattering wave function is expanded on a basis of 289 states dissociating at large hyper-radius into the H_2 (16, 14, 10, 8, 0) and SH (44, 41, 38, 34, 31, 26, 21, 15, 1) rovibrational sets (this notation indicates the largest rotational level j for each vibrational manifold $v = 0-4$ for H_2 and $v' = 0-8$ for SH). The coefficients of the expansion satisfy a set of second-order-coupled differential equations with couplings arising from the difference between the exact Hamiltonian and the reference Hamiltonian. These coupled equations are solved using the Johnson−Manolopoulos log-derivative propagator.[26] The number of coupled equations increases from 289 for $J = 0$ to 4706 for $J = 32$.

QM scattering calculations of insertion reactions are more difficult than those of abstraction reactions for two main reasons. First, the PES presents a deep well (96 kcal/mol in the present case), and thus many states have to be considered in the close-coupling equations. The number of states is a crucial parameter for convergence. Second, in the S(^{1}D) + H_2 reaction, symmetric top configurations (where the Coriolis coupling is large) lie near the HSH potential minimum and are thus energetically accessible. Therefore, we have to include all allowed Ω components (where Ω is the projection of the total angular momentum J on the axis of least inertia) in the close-coupling expansion states to obtain accurate integral and differential cross sections. In addition, the asymptotic matching distance (which is another crucial parameter for convergence) used for the title reaction is larger than for other insertion reactions already studied using this method.

By use of this methodology, we have computed integral and differential cross sections for the S(^{1}D) + H_2 ($v = 0$, $j = 0$, 1) reactions at the collision energy of 2.24 kcal/mol. In addition, QM reaction probabilities at total angular momentum $J = 0$ for the S(^{1}D) + H_2 ($v = 0$, $j = 0$) reaction have been calculated in a regular grid of collision energies between 0 and 11.5 kcal/mol.

The QCT calculations have been performed by running batches of 10^5 trajectories at 2.24 and 3.96 kcal/mol collision energies and H_2($v = 0$) in the rotational levels $j = 0$ and 1 following the procedures described in detail elsewhere.[27] The integration step size in the trajectories was chosen to be 5×10^{-17} s. This guarantees a total energy conservation better than one part in 10^4 and conservation of total angular momentum better than one part in 10^6. The trajectories were started at a distance between the incoming atom and the center-of-mass of the diatomic of 7 Å. The rovibrational energies of the H_2 reagent and those of the SH product were calculated by semiclassical quantization of the action using the potential given by the asymptotic diatom limits of the PES. These rovibrational energies were fitted to Dunham expansions containing 20 terms (fourth power in $v + {}^1/_2$ and third power in $j(j + 1)$). The assignment of product quantum numbers (v',j') is carried out by equating the classical rotational angular momentum of the product molecule to $[j'(j' + 1)]^{1/2}\hbar$. With the (real) j' value so obtained, the vibrational quantum number v' is found by equating the internal energy of the outgoing molecule to the corresponding Dunham expansion. In the most common procedure, these real v' and j' values are rounded to the nearest integer, hereafter, histogramatic binning (HB) method. However, this rounding procedure may cause important discrepancies between the classical and quantum internal energy distributions, especially in the case of slightly endoergic or nearly thermoneutral channels of a reaction. Moreover, rovibrational channels that are closed quantum mechanically can be classically accessible due to this rounding method. This may cause important distortions in the classical rotational distributions of the highest vibrational levels accessed by the products when compared with the QM ones, and the effect will be larger for those product molecules characterized by large vibrational and rotational spacings. As in our previous work,[12] we have implemented a Gaussian-weighted binning (GB) procedure, equivalent to that proposed by Bonnet and Rayez.[28] Briefly, a Gaussian function centered at the quantal action and with a given width has been used to weight the trajectories following the criteria that the closer the vibrational action of a given trajectory to the nearest integer, the larger the weighting coefficient for that trajectory. In particular, in the present work we have used a full-width-half-maximum for the Gaussian functions of 0.1. As it has been shown recently,[12] a much better agreement is obtained between the QM and QCT vibrational branching ratios and product rotational distributions when the GB procedure is employed in the QCT calculations. A similar procedure can be applied to the rotational action; however, the resulting cross sections and reaction probabilites are indistinguishable with those obtained without GB.

The collision energy evolution of the reaction probability at total angular momentum $J = 0$, $P^{J=0}(E_c)$, for the S(^{1}D) + H_2 ($v = 0$, $j = 0$) reaction has been calculated by running batches of 10^5 trajectories with a zero-impact parameter in the collision energy range 0.10−13.8 kcal/mol as described in ref 27. The calculation of the vibrational state-resolved reaction probabilities has been performed by the method of moments expansion in Legendre polynomials and employing the GB procedure commented on above to assign final vibrational states.

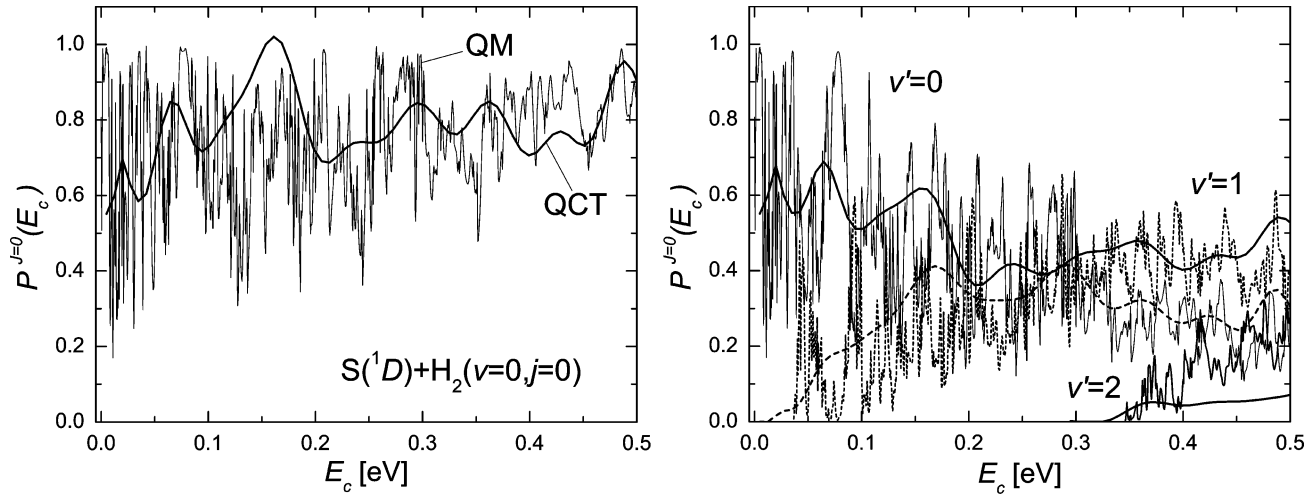

Figure 1. QM and QCT total (left panel) and vibrational state-resolved (right panel) reaction probabilites as a function of collision energy for total angular momentum $J = 0$ calculated for the $S(^1D) + H_2$ ($v = 0$, $j = 0$) reaction. The QCT results have been obtained using the GB method to assign product vibrational states.

As in previous works on the $O(^1D)$ + HD reaction,[29,30] the simulation of the experimental angle-selected product translational energy distributions $P(E'_t,\Delta\theta)$, where $\Delta\theta = \theta_2 - \theta_1$, was carried out using the equation

$$P(E'_t,\Delta\theta) = \sum_k N_k \exp\left[-\left(\frac{E'_t - E_k}{\Delta E_k}\right)^2\right] \int_{\theta_1}^{\theta_2} \left(\frac{1}{\sigma_R}\frac{d\sigma_R}{d\omega_k}\right) \sin\theta \, d\theta \quad (1)$$

where the sum extends to every rovibrational state $k = (v', j')$ of the SH product, E_k is the H-atom center-of-mass recoil energy corresponding to the SH internal state k, and $(d\sigma_R/d\omega)_k$ is the theoreticalv', j' state-resolved differential cross section.

The resolution of the experiment is modeled with a Gaussian function centered at E_k, with normalization constant N_k, and a width ΔE_k given by

$$\Delta E_k = \frac{2m_H M}{m_{SH}} w_k \Delta w \quad (2)$$

where m_H and m_{SH} are the masses of the H atom and SH product molecule and $M = m_S + m_{H2}$. The product recoil velocity resolution Δw is defined as

$$\Delta w = [\sin^2\theta \cos^2\phi \, (\Delta w_x)^2 + \sin^2\theta \sin^2\phi \, (\Delta w_y)^2 + \cos^2\theta \, (\Delta w_z)^2]^{1/2} \quad (3)$$

where Δw_x, Δw_y, and Δw_z are 750, 150, and 1100 ms^{-1}, respectively.[29]

III. Results and Discussion

A. Reaction Probabilities. Figure 1 presents the QM and QCT-GB total and vibrational state-resolved reaction probabilities at total angular momentum $J = 0$, $P^{J=0}(E_c)$, as a function of collision energy, E_c, for the $S(^1D) + H_2$ ($v = 0$, $j = 0$) reaction. The QM reaction probabilities show a dense resonance structure, especially at low collision energies, which corresponds to QM narrow resonances associated with the deep H_2S well in the PES. The total reaction probability is high (average values of about 0.7−0.8), do not show energy threshold, and is fairly constant with collision energy, as expected for a reaction with no barrier and a deep well. As can be seen in the right panel of Figure 1, as collision energy increases and the $v' = 1$ channel becomes energetically accessible, the reaction probability for $v' = 0$ declines. The QCT results reproduce quite satisfactorily the overall shape of the total and v' state-resolved QM reaction probabilities, although the QCT reaction probabilities for $v' = 2$ are significantly smaller than the QM ones. In addition, from the opening of the $v' = 2$ channel, the QCT $v' = 0$ reaction probabilities are somewhat larger than the QM ones, and those for $v' = 1$ are smaller.

Particularly interesting is the matching of the QM energy thresholds for $v' = 1$ and $v' = 2$ by the QCT calculations employing the present GB procedure. If the conventional HB method is used, then the QCT $v' = 1$ and $v' = 2$ energy thresholds are sensibly smaller than the QM ones. As expected, the QCT reaction probabilities do not show any sharp peak structure, although they show broad oscillations, which follow approximately the averaged QM reaction probabilities. The same degree of agreement between QM and QCT reaction probabilities has been found also for the $C(^1D) + H_2$ reaction.[12]

TABLE 1: QM and QCT Integral Cross Sections, σ, (in Å^2) for the $S(^1D) + H_2$ ($v = 0$, $j = 0$, 1) Reaction at 2.24 and 3.96 kcal/mol (only QCT values available) Collision Energies[a]

	total	$v' = 0$	$v' = 1$	v' branching ratio
		$E_c = 2.24$ kcal/mol		
QM $j = 0$	27.21	24.17	3.04	0.13
QCT-HB $j = 0$	24.28	20.40	3.88	0.19
QCT-GB $j = 0$	22.85	20.88	1.97	0.09
QM $j = 1$	27.42	23.63	3.79	0.16
QCT-HB $j = 1$	25.70	21.09	4.61	0.22
QCT-GB $j = 1$	24.45	21.55	2.90	0.13
		$E_c = 3.96$ kcal/mol		
QCT-HB $j = 0$	22.06	17.45	4.61	0.26
QCT-GB $j = 0$	21.76	18.01	3.74	0.21
QCT-HB $j = 1$	22.14	17.30	4.84	0.22
QCT-GB $j = 1$	21.99	17.88	4.11	0.23

[a] In the QCT case, the results obtained using the HB and GB procedures are shown. The vibrational branching ratio is defined as $\sigma(v' = 1)/\sigma(v' = 0)$.

B. Integral Cross Sections and Product Rotational Distributions. The QM and QCT total and v' state-resolved integral cross sections (ICS) for the $S(^1D) + H_2$ ($v = 0$, $j = 0$, 1) reaction calculated at 2.24 and 3.96 kcal/mol collision energies are presented in Table 1. The total QCT ICSs calculated using either of the two binning methods, QCT-HB and QCT-GB, at 2.24

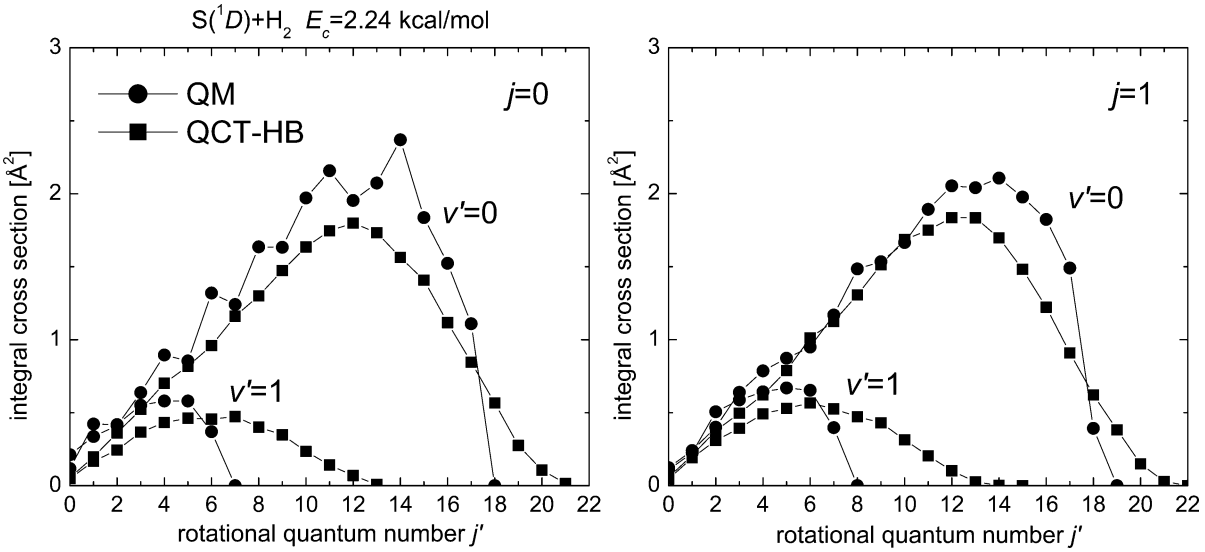

Figure 2. QM and QCT vibrational state-resolved integral cross sections calculated for the S(^{1}D) + H_2 ($v = 0$, $j = 0$, 1) reaction at $E_c = 2.24$ kcal/mol. Left panel: $j = 0$. Right panel: $j = 1$. The QCT results have been obtained using the usual HB method to assign product quantum states.

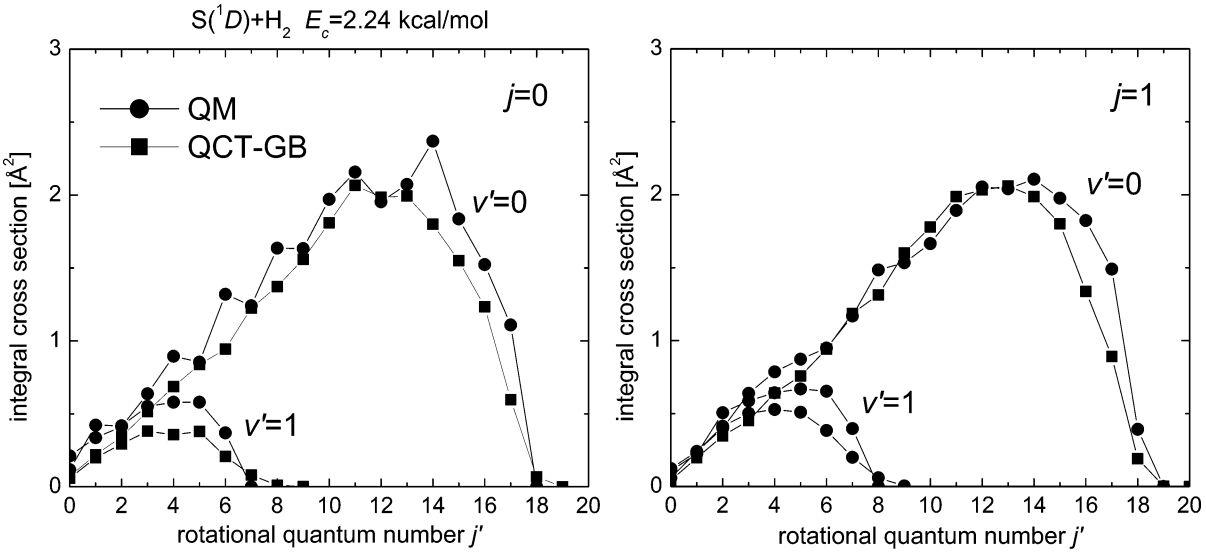

Figure 3. Same as Figure 2 but in this case the QCT results have been obtained using the GB method to assign product quantum states.

kcal/mol collision energy are smaller than the QM cross sections, especially for initial $j = 0$. In addition, the QCT-GB ICSs are somewhat smaller than the QCT-HB ones. More interesting is the comparison between the vibrational state-resolved ICSs, especially for the reaction yielding SH($v' = 1$). The QCT-HB method overestimates the QM cross sections in this particular vibrational state. However, the cross sections obtained when using the QCT-GB method are smaller than the QM ones. The QCT-GB vibrational branching ratios, calculated as $\sigma(v' = 1)/\sigma(v' = 0)$ (see Table 1) are in better agreement with the QM ones than those obtained using the QCT-HB method. At the higher collision energy of 3.96 kcal/mol, no QM calculations are available and the differences between QCT-HB and QCT-GB ICSs and vibrational branching ratios are much smaller than at the lower collision energy.

The comparison between the QM and QCT SH(v') product rotational distributions for the S(^{1}D) + H_2 ($v = 0$, $j = 0$, 1) reactions calculated at 2.24 kcal/mol are presented in Figures 2 and 3. The QCT results shown in Figure 2 correspond to the HB method, and those obtained using the GB method are depicted in Figure 3. At this collision energy, the rotational distributions predicted by the QM calculations peak at about $j' = 15$ and $j' = 5$ for $v' = 0$ and $v' = 1$, respectively. As expected, the QCT-HB v' state-resolved rotational distributions are hotter than their QM counterparts, and the distributions reach j' values beyond those allowed quantum mechanically, especially for the highest SH vibrational state $v' = 1$. In contrast, the rotational distributions obtained by the QCT-GB method (see Figure 3) agree quite well with the QM distributions, both in shape and maximum j' value allowed for every vibrational state. The remaining discrepancies between the QCT-GB and QM distributions are related with the smaller value of the v' QCT ICSs.

The QCT-HB and QCT-GB rotational distributions calculated at the higher 3.96 kcal/mol collision energy are shown in Figure 4. At this collision energy, the QCT-HB rotational distributions are also hotter, especially for SH($v' = 1$). Although no QM results are available at this collision energy, it is expected a similar degree of agreement between QCT-GB and QM as that found at 2.24 kcal/mol.

The same degree of agreement between QM and QCT-GB rotational distributions has been found recently also for the insertion reaction C(^{1}D) + H_2.[12] The QCT-GB procedure followed in this and previous works seems to be quite reliable in reproducing the shape of the rotational distributions and the

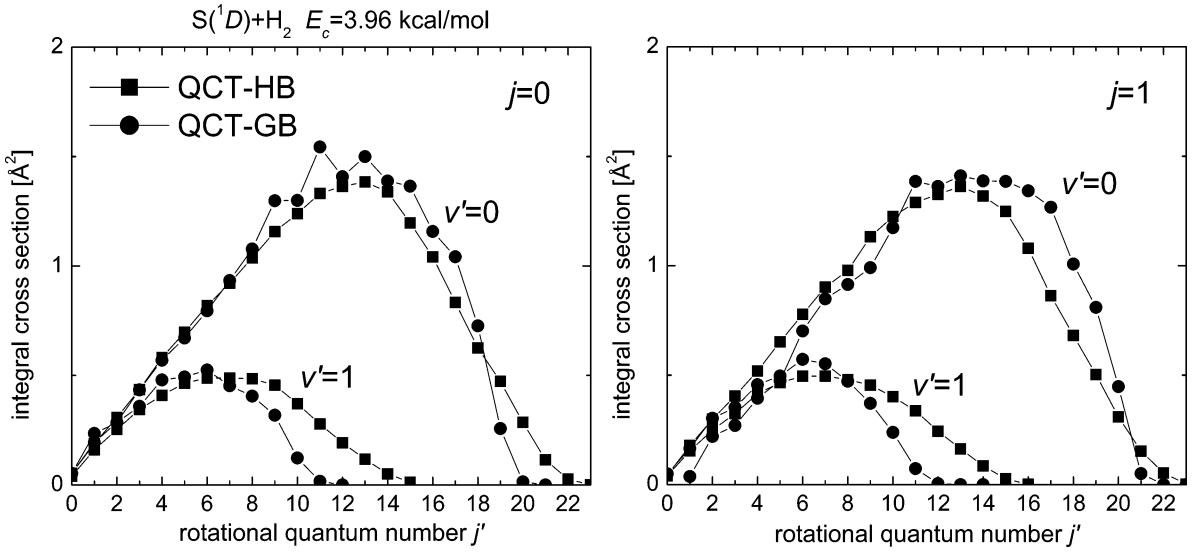

Figure 4. QCT-HB and QCT-GB vibrational state-resolved integral cross sections calculated for the $S(^1D) + H_2$ ($v = 0$, $j = 0$, 1) reaction at $E_c = 3.96$ kcal/mol. Left panel: $j = 0$. Right panel: $j = 1$. No QM calculations are available at this collision energy.

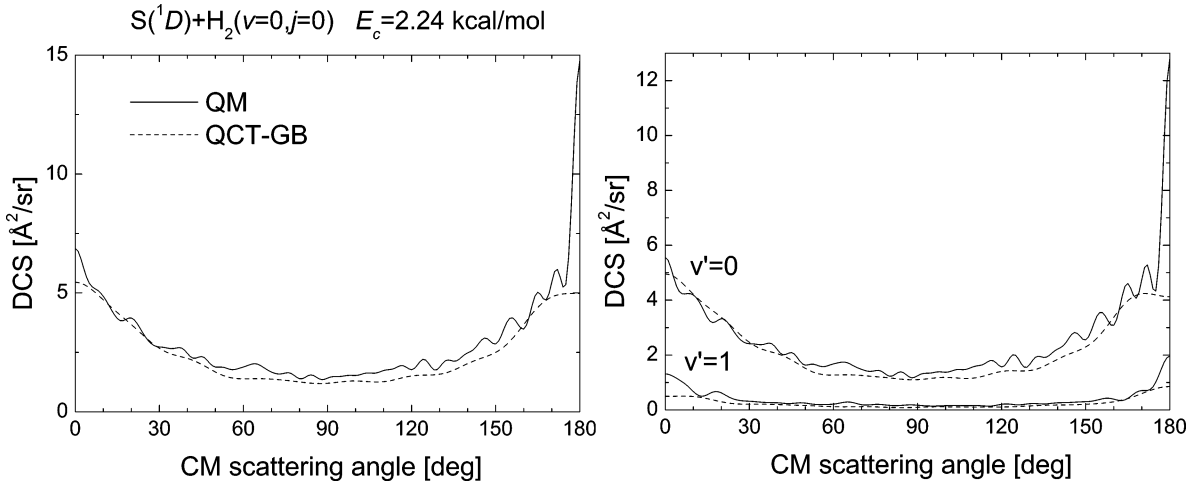

Figure 5. QM and QCT-GB total (left panel) and vibrational state-resolved (right panel) differential cross sections calculated for the $S(^1D) + H_2$ ($v = 0$, $j = 0$) reaction at $E_c = 2.24$ kcal/mol.

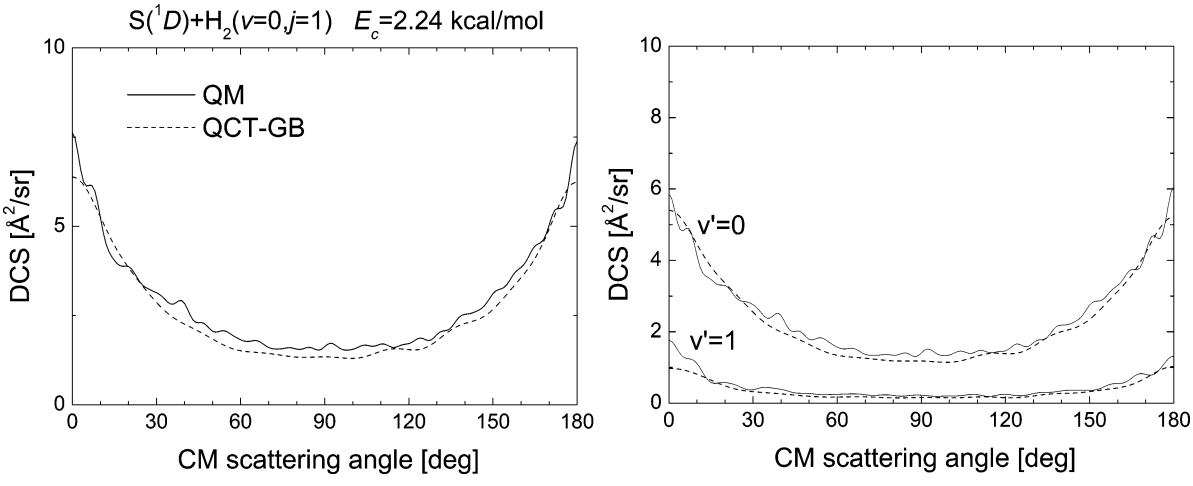

Figure 6. Same as Figure 5 but for the $S(^1D) + H_2$ ($v = 0$, $j = 1$) reaction.

maximum value of j' allowed for every product v' state obtained in accurate QM calculations for the insertion reactions. Moreover, the method has proved to be quite robust also for abstraction reactions.[31] Given the good performance of the QCT-GB method, in the remaining of the paper we will present and discuss only comparisons between QCT-GB and QM results.

C. Differential Cross Sections and Product Translational Energy Distributions. Figures 5 and 6 show the total and vibrational state-resolved differential cross sections (DCS) for the reaction with H_2 in $j = 0$ and $j = 1$, respectively, calculated at 2.24 kcal/mol collision energy. The total QM DCSs are backward−forward symmetric, showing a sharp peak at scat-

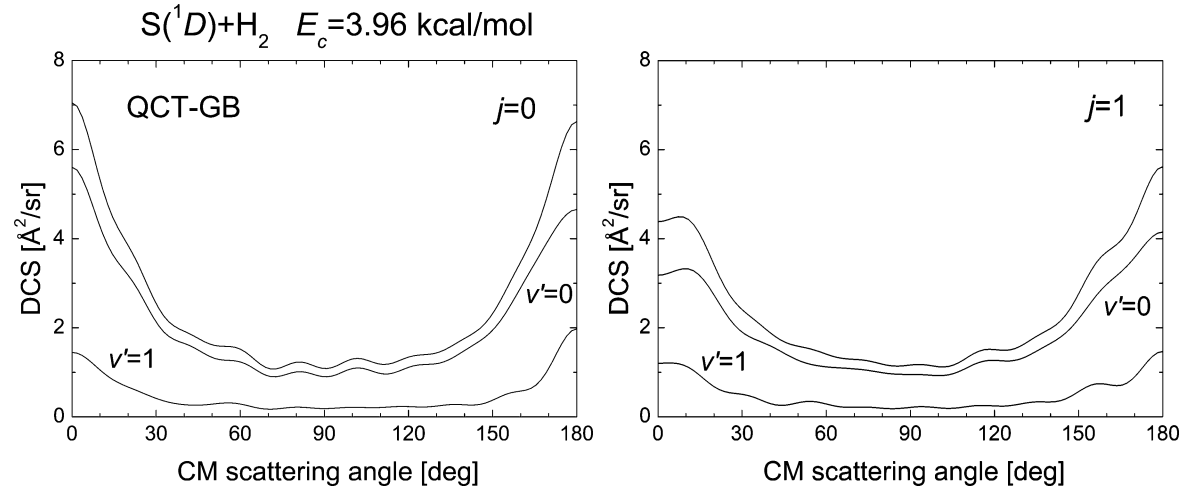

Figure 7. QCT-GB total and vibrational state-resolved differential cross sections for the S(¹D) + H_2 ($v = 0$, $j = 0$) (left panel) and S(¹D) + H_2 ($v = 0$, $j = 1$) (right panel) reactions at $E_c = 3.96$ kcal/mol.

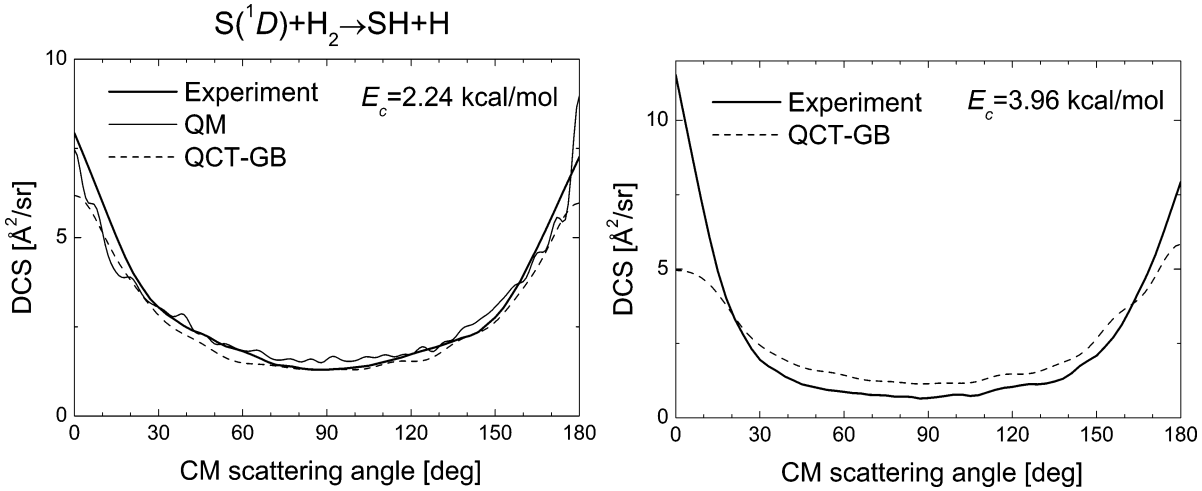

Figure 8. Comparison between experimental and theoretical total differential cross section for the S(¹D) + H_2 reaction. Left panel: $E_c = 2.24$ kcal/mol. Right panel: $E_c = 3.96$ kcal/mol. Thick solid curve: experimental results from ref 14. Thin solid line: QM calculation. Dashed line: QCT-GB calculation.

tering angles close to 180° (extreme backward) for the reaction with H_2 in $j = 0$ (see left panel of Figure 5). The corresponding QCT-GB total DCSs are depicted in the same figures by dashed curves. The agreement between QM and QCT-GB is quite good in most of the scattering angular range, with the exception of the extreme backward angles of the reaction with H_2 in $j = 0$, where the QCT results do not reproduce the sharp peak found in the QM case. The good agreement between QCT-GB and QM for total DCSs extends to the v' state-resolved DCSs. The examination of the v' state-resolved DCSs indicates that the extreme backward QM peak is associated with SH($v' = 0$) products.

The total and v' state-resolved QCT-GB DCSs calculated at 3.96 kcal/mol for the reactions with H_2 in $j = 0$ and $j = 1$ are shown in Figure 7. At this collision energy, no QM calculations are available, but a similar degree of agreement between the present QCT-GB results and the QM ones is expected. As for the lower collision energy, the DCS are nearly backward−forward symmetric, with some propensity for backward in the case of the reaction with initial $j = 1$.

The total DCSs presented in Figures 5−7 have been used to simulate the experimental results measured by Liu and co-workers,[14] which include total and angle-resolved product translational energy distributions and angular distributions for the title reaction. In the crossed-beam experiments of Liu and co-workers, the H_2 molecules have a rotational temperature of about 150 K. The relative weights of the different rotational states of H_2 are then 0.216, 0.744, 0.034, and 0.006 for the $j = 0-3$ rotational states. To simulate the experimental conditions with the calculations carried out in this work, we have considered the weights 0.216 and 0.784 for $j = 0$ and $j = 1$, respectively. Figure 8 shows the comparison between the experimental angular distribution and those obtained theoretically at the collision energies 2.24 kcal/mol (left panel) and 3.96 kcal/mol (right panel). The experimental angular distributions have been scaled to have the same area as the QM one at $E_c = 2.24$ kcal/mol and as the QCT-GB at $E_c = 3.96$ kcal/mol. The agreement found at $E_c = 2.24$ kcal/mol between experiment and theory is nearly quantitative. The QM DCS does not show the sharp peak at the extreme backward scattering once the averaging in initial H_2 rotational states is performed. The agreement found at the $E_c = 3.96$ kcal/mol between experiment and QCT-GB (no QM results are available) is less satisfactory. The experimental DCS shows a propensity for forward scattering and a large polarization between backward/forward and sideways scattering, whereas the QCT-GB DCS is backward−forward symmetric showing less polarization.

Figure 9 shows the simulation of the total product translational energy distribution $P(E'_t)$ for the title reaction at $E_c = 2.24$ kcal/mol using the QCT-GB (left panel) and QM (right panel)

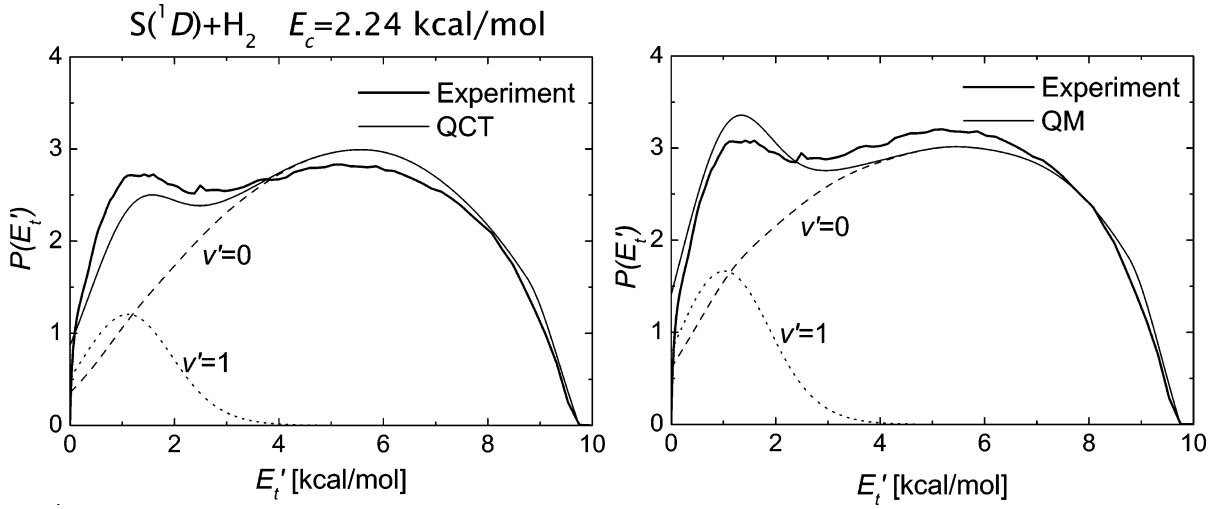

Figure 9. Comparison between experimental and theoretical total and vibrational state-resolved product translational energy distributions for the $S(^1D) + H_2$ reaction at $E_c = 2.24$ kcal/mol. Left panel: experiment vs QM. Right panel: experiment vs QCT-GB. Thick solid curve: experimental results from ref 14. Thin solid line: QM or QCT-GB calculations. Dashed line: SH($v' = 0$). Dotted line: SH($v' = 1$).

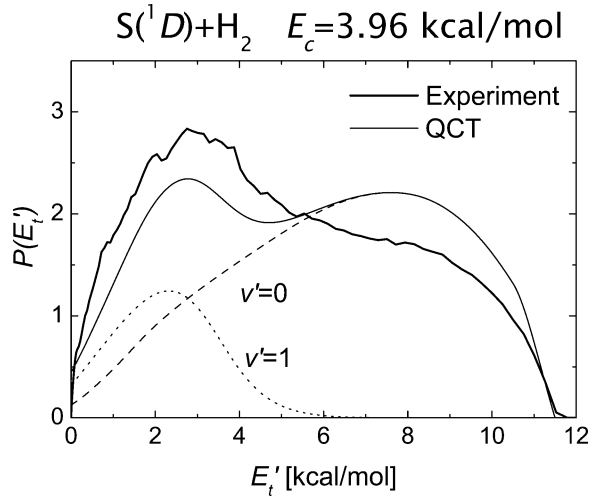

Figure 10. Same as Figure 9 but for the $S(^1D) + H_2$ reaction at $E_c = 3.96$ kcal/mol. In this case, no QM calculations are available.

results. In both cases, the experimental distribution has been normalized to the same area as the theoretical ones. The relative contributions from products in $v' = 0$ and $v' = 1$ obtained theoretically are also depicted. From the simulations, it is clear that the broad double-peak structure of the experimental $P(E'_t)$ is associated with the reaction yielding SH molecules in $v' = 0$ and $v' = 1$. The shape of the experimental $P(E'_t)$ is well reproduced by the theoretical simulations with some small discrepancies. The most important difference between the QM and QCT-GB simulations is in the relative contribution of $v' = 1$ with respect to $v' = 0$. As seen in Table 1, the QCT-GB vibrational branching ratio is smaller than the QM one and this explains the different height of the first and second broad peaks in the $P(E'_t)$ with maxima at about $E'_t = 1$ kcal/mol and $E'_t = 5$ kcal/mol in both the QCT-GB (first peak smaller than the second) and QM (first peak higher than the second). The experimental $P(E'_t)$ lies between, with similar heights of the $v' = 0$ and $v' = 1$ peaks, suggesting a vibrational branching ratio between the QM and QCT-GB ones.

The QCT-GB simulation of the experimental $P(E'_t)$ at $E_c = 3.96$ kcal/mol is shown in Figure 10. At this collision energy, the agreement between theory (QCT-GB only) and experiment is worse. The experimental $P(E'_t)$ shows a first peak at about $E'_t = 3$ kcal/mol followed by a smooth decline with a broad maximum peaking at $E'_t \approx 8$ kcal/mol. This indicates that experimentally the vibrational branching ratio at this collision energy is significantly larger than at $E_c = 2.24$ kcal/mol. The QCT-GB calculation clearly underestimate the vibrational branching ratio observed experimentally, as it is evident from the theoretical $P(E'_t)$, where the broad peaks associated with the $v' = 0$ and $v' = 1$ product states have similar heights.

A more stringent test of the accuracy of the present theoretical results for this insertion reaction can be obtained from the comparison with the angle and vibrational state-specific product translational energy distributions deduced by Lee and Liu.[14] Figures 11 and 12 show the comparison between the experimental $P(E'_t,\Delta\theta)$ and the QM and QCT-GB simulations, respectively, at $E_c = 2.24$ kcal/mol. The experimental distributions in Figures 11 and 12 have been scaled to the QM ones using a single scaling factor. This scaling factor has been obtained from the data at the scattering angle range 45−60° (see right-hand top panel of Figure 11) by making sure that the area of the experimental curve coincides with that of the QM curve. As can be seen, there is a good general agreement between both theoretical simulations and the experimental data for the different ranges of scattering angles. The shapes of the broad distributions are well reproduced in general, with the exception of the range of sideways scattering angles (75−90° and 90−105°), especially in the QM case, where the theoretical simulations predict significant more population at $E'_t > 5$ kcal/mol than the experimental distributions. The experimentally deduced partitioning into vibrational states $v' = 0$ and $v' = 1$ agrees qualitatively with the theoretical predictions in most cases. Again, the main difference between the QM and QCT-GB simulations is associated with the smaller v' branching ratio found in the QCT calculations in comparison with the QM ones.

The QCT-GB simulations of the $P(E'_t,\Delta\theta)$ obtained at $E_c = 3.96$ kcal/mol are compared with the experimental distributions in Figure 13. It must be emphasized that the experimental $P(E'_t,\Delta\theta)$ have been scaled to the theoretical ones using the same scaling factor obtained at $E_c = 2.24$ kcal/mol as indicated above. As in the cases of the angular distribution and total $P(E'_t)$, the agreement at this collision energy is less satisfactory for the angle-specific translational energy distributions. The shape of the measured distributions and the partitioning into product vibrational states are only qualitatively reproduced by the QCT-GB calculations. There are large discrepancies, especially at the

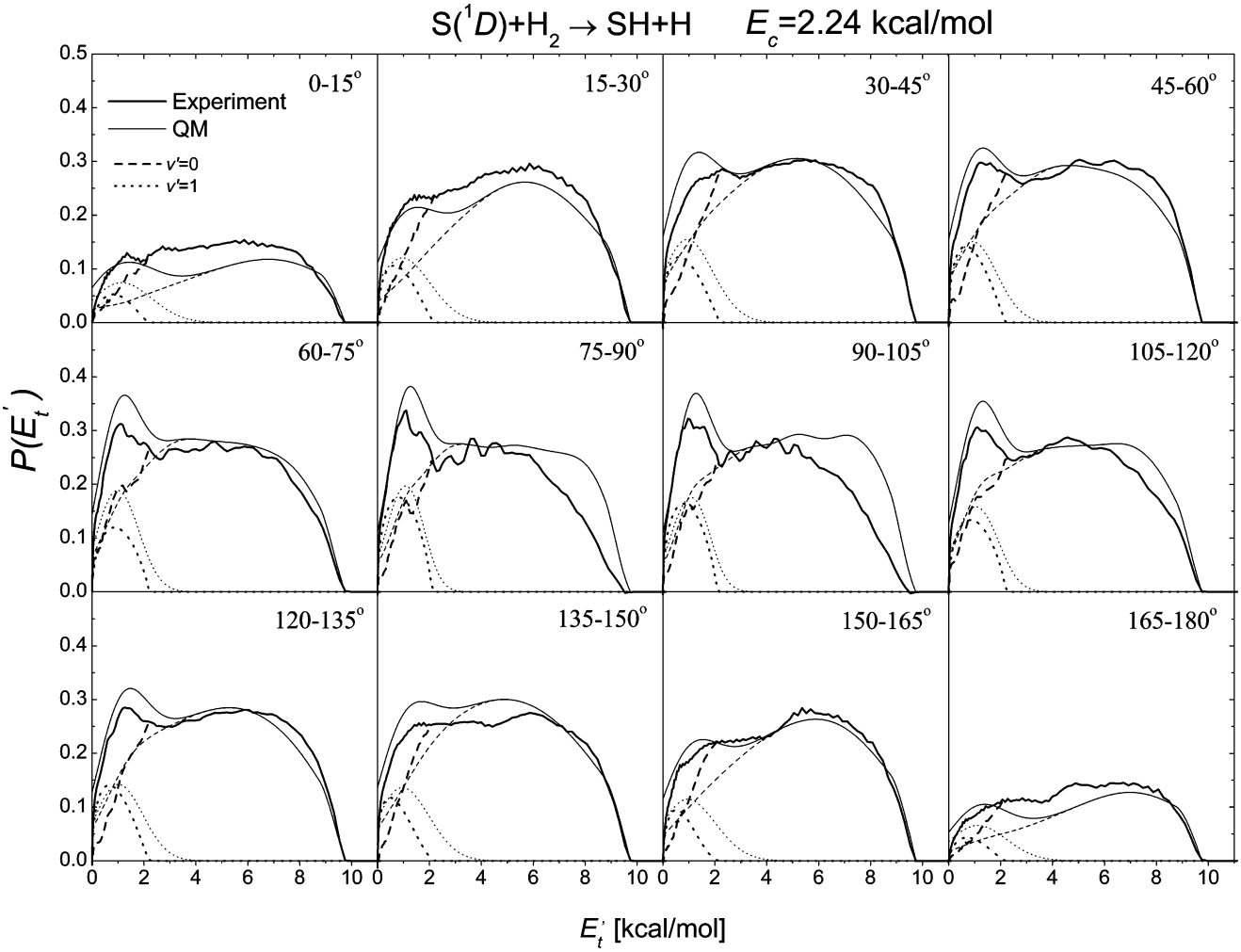

Figure 11. Scattering angle-selected total and vibrational state-resolved product translational energy distributions, $P(E'_t,\Delta\theta)$, for the S(^{1}D) + H_2 reaction at E_c = 2.24 kcal/mol. Thick curves: experimental results from ref 14. Thin curves: QM simulations. The scaling between QM and experiment has been performed as indicated in the text for the data corresponding to $\Delta\theta = 45-60°$.

forward- and backward-scattering angles, where the QCT-GB underestimates the experimental distributions over all E'_t values and at sideways-scattering angles where the QCT-GB distributions overestimate the experimental one at $E'_t > 4-6$ kcal/mol.

Figure 14 depicts the experimental and theoretical scattering angle-specific vibrational branching ratios. The vibrational branching ratios have been calculated by dividing the areas under the $v' = 1$ curves in Figures 11−13 by those under the $v' = 0$ curves at each scattering angle interval. The indirectly deduced experimental vibrational branching ratios show maxima at sideways-scattering angles, the maximum being very much pronounced at $E_c = 3.96$ kcal/mol. At this last collision energy, there is also a large peak at the 150−165° interval, which seems to be somewhat anomalous. These experimental maxima in the vibrational branching ratios would indicate that there is more vibrational excitation in sideways-scattered products than in those scattered in forward and backward. However, both QM and QCT-GB results at $E_c = 2.24$ kcal/mol and the QCT-GB ones at $E_c = 3.96$ kcal/mol show the opposite behavior; i.e., there is somewhat more vibrational excitation in forward and backward than in sideways, and at the higher collision energy, the branching ratio is nearly independent of the scattering angle. The total vibrational branching ratios experimentally deduced are 0.089 and 0.194 at $E_c = 2.24$ kcal/mol and $E_c = 3.96$ kcal/mol, respectively. In contrast, the theoretical values are always larger; at $E_c = 2.24$ kcal/mol, the QM value is 0.15 and the QCT-GB value is 0.12, and at $E_c = 3.96$ kcal/mol, the QCT-GB value is 0.23. This indicates that the analysis employed in ref 14 to infer the relative contributions of $v' = 0$ and $v' = 1$ to the $P(E'_t,\Delta\theta)$ is not exempt of some ambiguity and, thus, the conclusion obtained in the experimental work that the sideways scattering is characterized by a higher vibrational excitation in comparison with forward and backward must be taken with caution.

The worse agreement found between theory and experiment at the higher collision energy $E_c = 3.96$ kcal/mol is somewhat surprising, given the excellent agreement showed at the lower collision energy $E_c = 2.24$ kcal/mol. The larger polarization observed experimentally in the angular distribution as collision energy increases is clearly at variance with the present QCT-GB calculations. In addition, in the experiments carried out for other isotopic variants of the title reaction, such as S(^{1}D) + D_2 and S(^{1}D) + HD, this effect is milder or just the opposite.[17] Moreover, for the O(^{1}D) + H_2 reaction, the QM total DCS does not show more polarization as the collision energy increases from 1.29 kcal/mol to 2.31 kcal/mol.[24] From the comparisons between theory and experiment shown in Figures 11−13, it is evident that the theoretical calculations predict a higher product yield at $E'_t > 4-5$ kcal/mol at sideways scattering angles. This effect, which is more pronounced and extends to more scattering angle intervals at $E_c = 3.96$ kcal/mol (see Figure 13), may be responsible for the larger polarization in the angular distribution experimentally deduced and might be caused by a fly out of

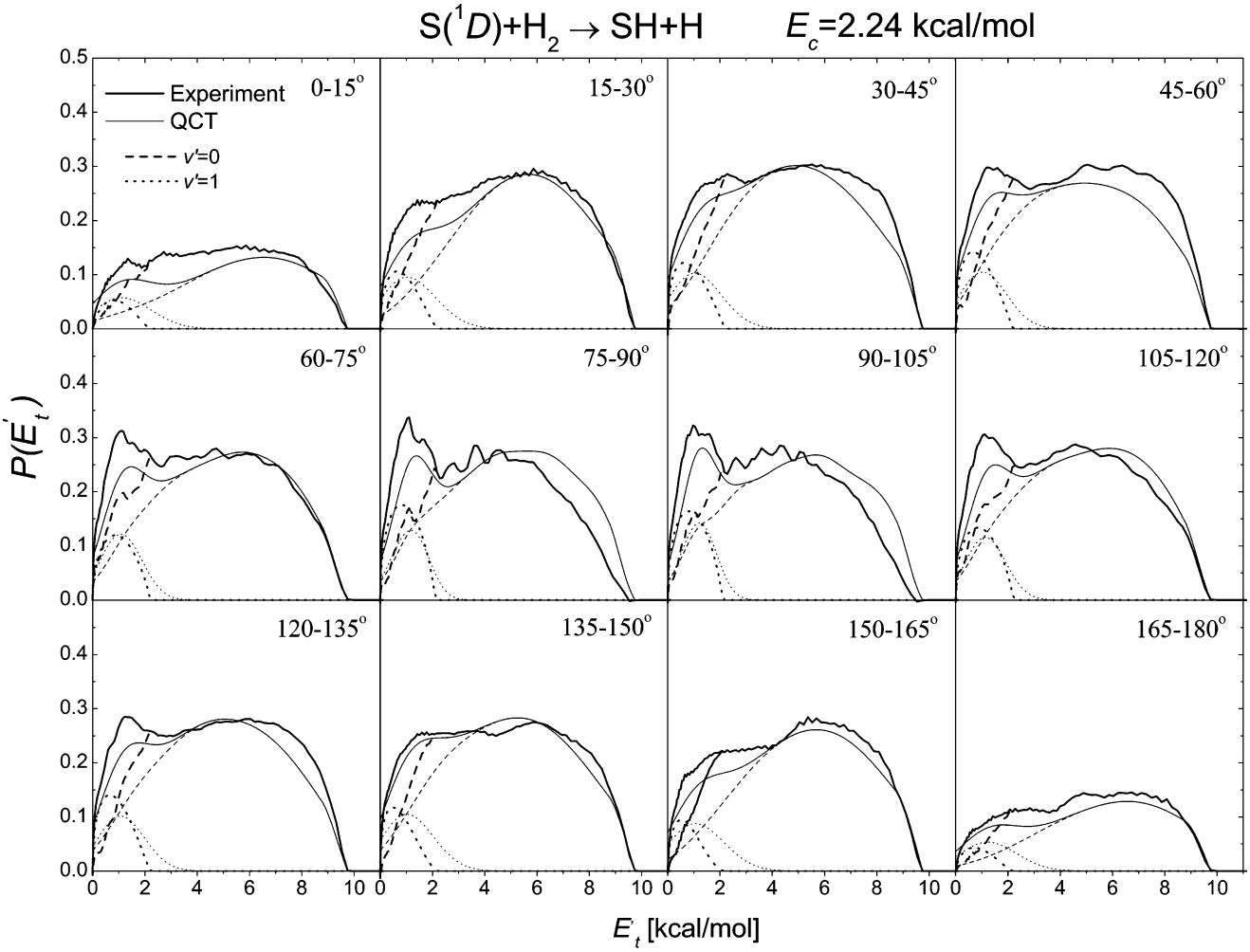

Figure 12. Same as Figure 11, but the theoretical simulations are now based on the QCT-GB calculations. The scaling between QCT-GB and experiment has been performed using the same scaling factor as in Figure 11.

fast H atoms from the detection region in the crossed-beam experiments.

Lee and Liu also presented in his work[14] three-dimensional (3D) representations of the gross features of the fully v', j' state-resolved DCSs deduced from the $P(E'_t,\Delta\theta)$ at both collision energies. Given the sin θ term included in the representations, an isotropic distribution would appear as sideways peaking, whereas a flat-top representation would correspond to forward−backward peaking distributions in the conventional representation for angular distributions. Lee and Liu found that, for $v' = 0$, the 3D representation was characteristic of a backward−forward peaking distribution. However, for $v' = 1$ the results indicated a much less polarized angular distribution, with a tendency to an isotropic distribution. The corresponding theoretical results obtained in the present work at $E_c = 2.24$ kcal/mol are depicted in Figure 15. As can be seen, the QM and QCT-GB results are in a rather good agreement, showing in all cases flat-top representations for both product vibrational states. As discussed in ref 14, a flat-top representation, i.e., a forward−backward peaking angular distribution, would correspond to the case where $L \approx L'$ for a reaction characterized by the formation of an intermediate complex. From the theoretical results presented here, this propensity holds for both the $v' = 0$ and $v' = 1$ states, at variance with the conclusions of Lee and Liu, who attributed a $\mathbf{L} \approx j'$ propensity for the products in $v' = 1$, based on the deduced sideways-peaking distribution.

D. Opacity Functions and Collision Times. An important piece of information in the comparison between the QM and QCT-GB calculations is the dependence of the reaction probability with the impact parameter, i.e., the opacity function. Figure 16 shows the total and vibrational state-resolved QM and QCT-GB degeneracy-weighted reaction probabilities as a function of the orbital angular momentum L, $(2L + 1)P(L)$ (at $j = 0$, also total angular momentum J), for the reactions with H_2 in $j = 0$ and $j = 1$. A good general agreement is found between both theoretical methods. In particular, the falloff of the opacity function at the largest L values observed in the QM case is well reproduced by the QCT-GB calculations. However, the classical reaction probabilities in the range $20 \leq L \leq 28$ for both $j = 0$ and $j = 1$ are smaller than the QM ones, especially for $j = 0$. This lack of reactivity in the QCT-GB case is related with the SH($v' = 0$) products.

Figure 17 shows the comparison between the QM and QCT-GB DCSs for the reactions with H_2 in $j = 0$ and $j = 1$ as a function of the L_{max} value retained in the partial wave sum. Similar to the $N(^2D) + H_2$ reaction,[10] all L values contribute to generate scattering in the whole angular range. The QCT-GB calculations reproduce the QM results quite well, with the exception of the extreme backward and forward regions, where the QM results show sharper peaks than the QCT-GB ones for all values of L_{max}, especially for the backward in the $j = 0$ reaction. Moreover, the narrow backward peak observed in the QM DCS for the reaction with $j = 0$ is clearly enhanced for $L \geq 20$. Therefore, a correlation is found between the lack of classical reactivity in the $20 \leq L \leq 28$ range of the opacity function and the appearance of the strong backward peak in

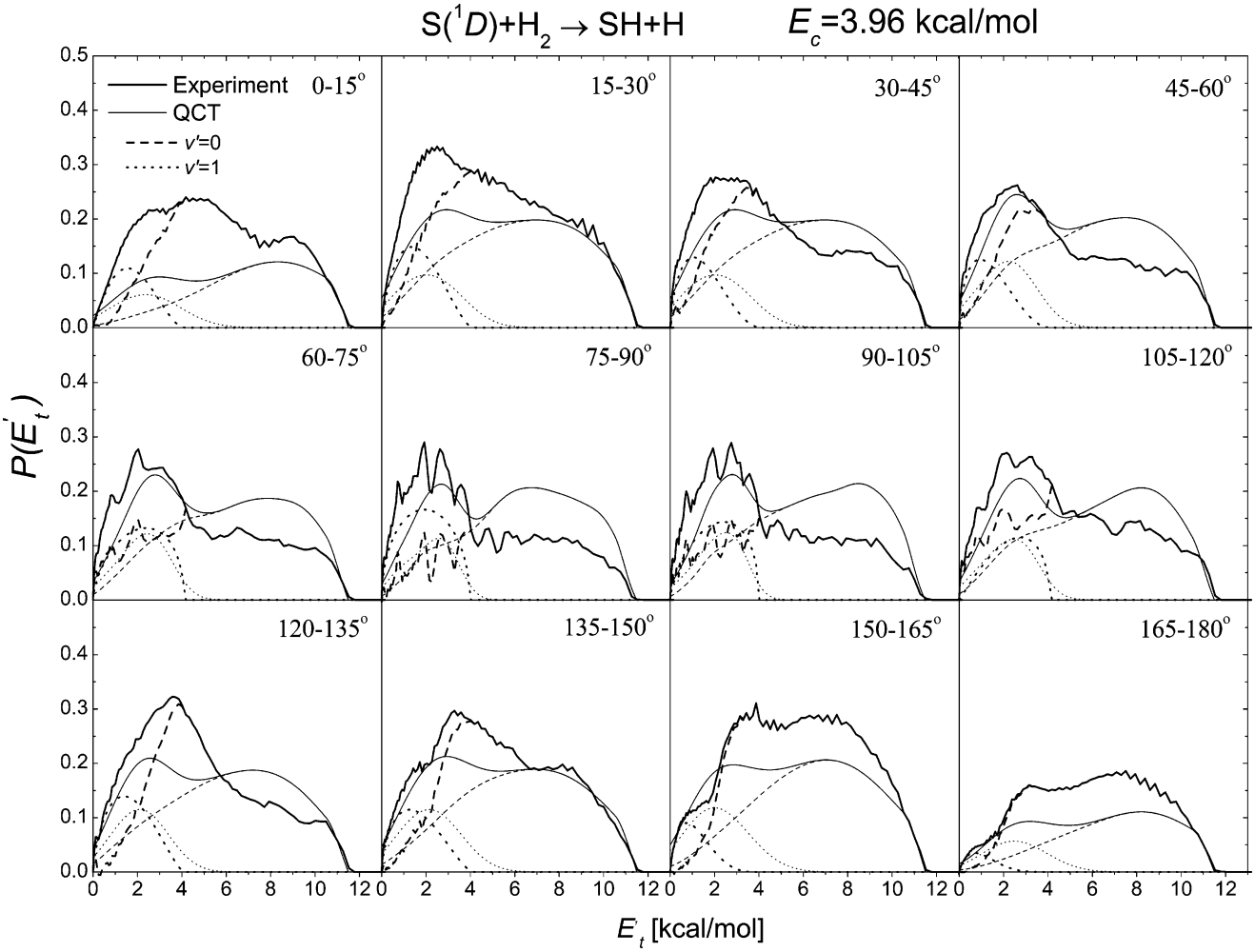

Figure 13. Same as Figure 11, but at $E_c = 3.96$ kcal/mol. The theoretical simulations are based on the QCT-GB calculations. No QM calculations are available at this collision energy. The scaling between QCT-GB and experiment has been performed using the same scaling factor as in Figure 11.

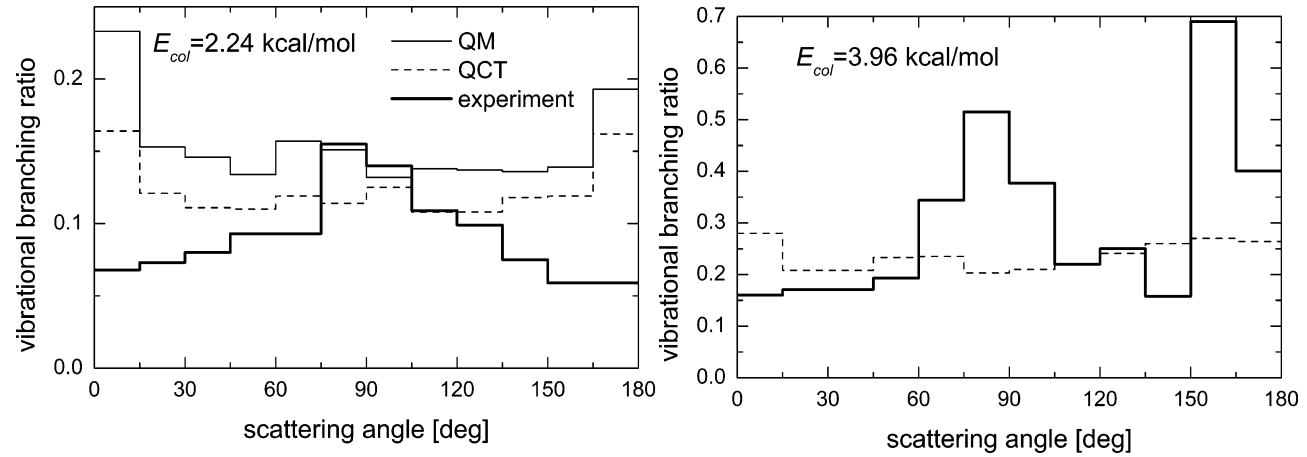

Figure 14. Comparison between experimental and theoretical (QM and QCT-GB) scattering angle-selected vibrational branching ratios, for the title reaction at $E_c = 2.24$ (left panel) and 3.96 kcal/mol (right panel). The vibrational branching rations have been calculated by dividing the areas under the $v' = 1$ curves by those under the $v' = 0$ curves at each scattering angle interval.

the QM DCS, suggesting that this is a genuine QM effect. Interestingly, the peak only appears in backward scattering, being much smaller in the forward region. Notice that for this reaction the largest L values for which there is reaction in the QM case are also reached in the QCT-GB calculations. Thus, it is not clear that this QM effect can be related with the existence of tunneling through the reactant and product centrifugal barriers at the very highest values of the angular momenta contributing to reaction.

All the attributes presented in this work for the title reaction are typical of an insertion mechanism. One way to analyze the degree of correlation between the insertion mechanism and the formation of a long-lived intermediate complex is by calculating the collision times of the trajectories, in other words, the time

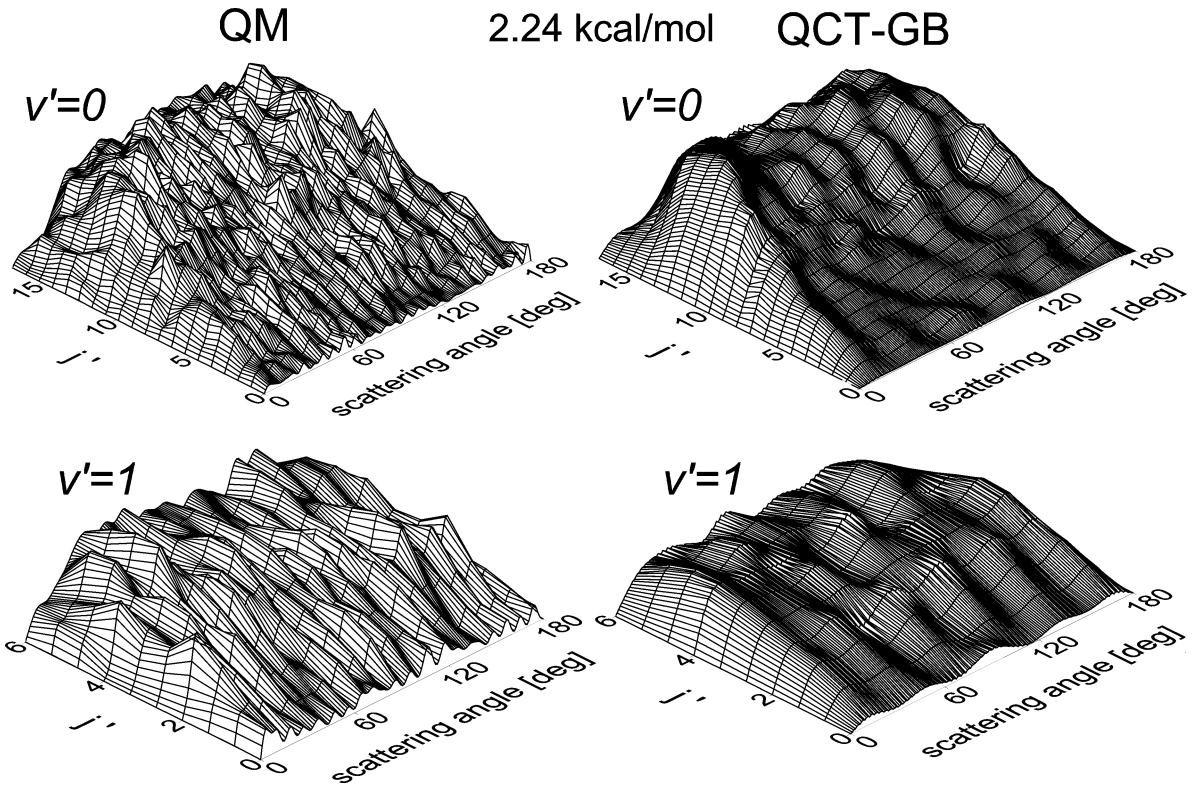

Figure 15. 3D plots of the rotationally state-resolved differential cross sections for the $S(^1D) + H_2$ reaction at $E_c = 2.24$ kcal/mol. Top: $v' = 0$. Bottom: $v' = 1$. Left: QM. Right: QCT-GB.

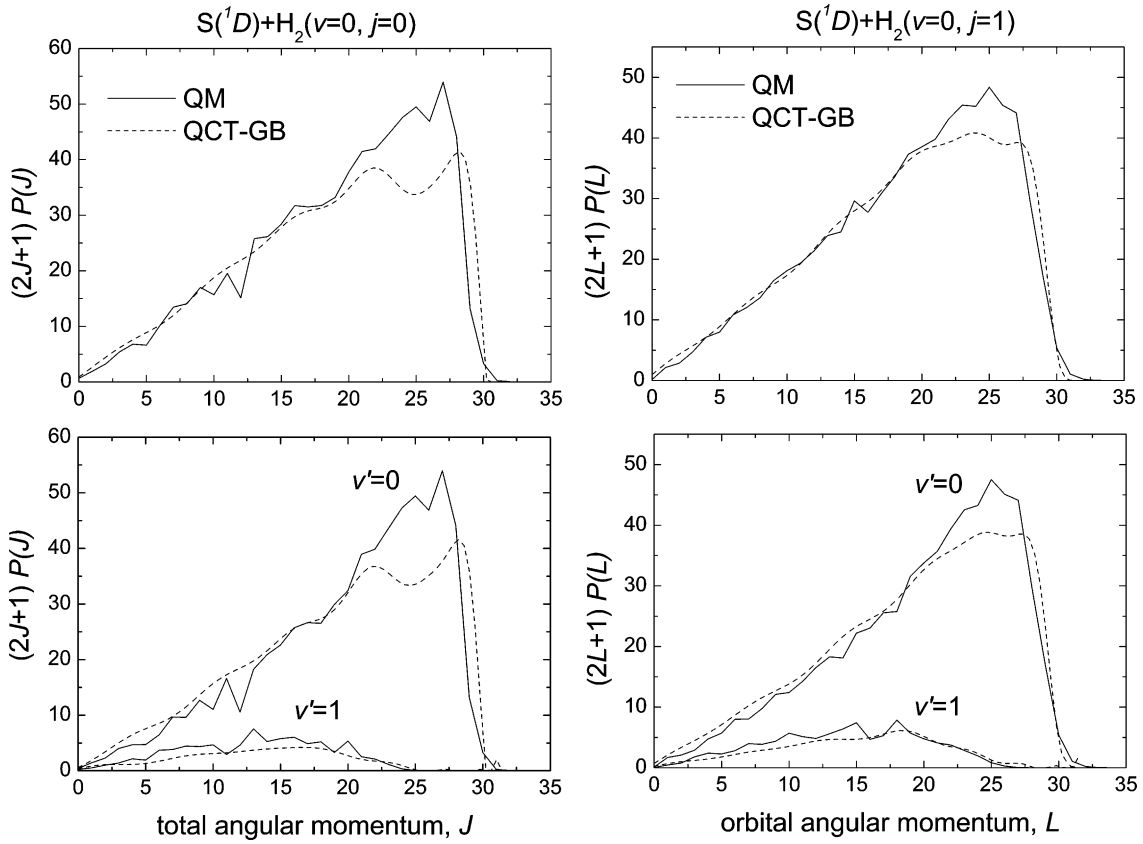

Figure 16. QM and QCT-GB total and vibrational state-resolved degeneracy-weighted opacity functions for the reactions of $S(^1D)$ and H_2 molecules in $j = 0$ (left panels) and $j = 1$ (right panels) at $E_c = 2.24$ kcal/mol.

elapsed between the strong interaction in the entrance and exit channels of the reaction. The analysis of the collision times allows us to get more insight into the detailed mechanism of the reaction, since the collision time can be taken as a measurement of the classical lifetime of the collision complex. In this work, we have calculated the collision time, τ_c, as $\tau_c =$

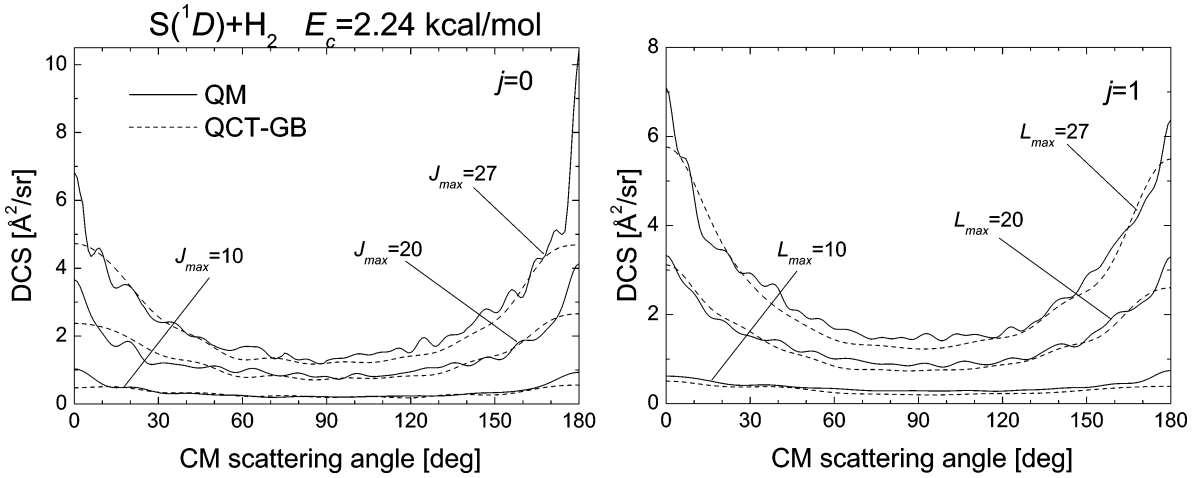

Figure 17. QM and QCT-GB differential cross sections as a function of the maximum orbital angular momentum L_{max} retained in the partial wave sum for the S(^{1}D) + H_2 ($v = 0$, $j = 0$, 1) reactions at $E_c = 2.24$ kcal/mol. Left panel: $j = 0$. Right panel: $j = 1$.

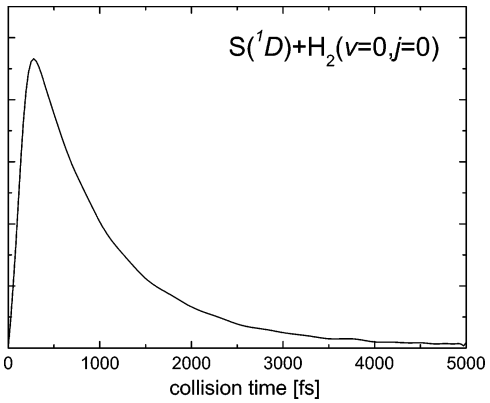

Figure 18. Distribution of classical collision times calculated for the S(^{1}D) + H_2 ($v = 0$, $j = 0$) reaction at $E_c = 2.24$ kcal/mol.

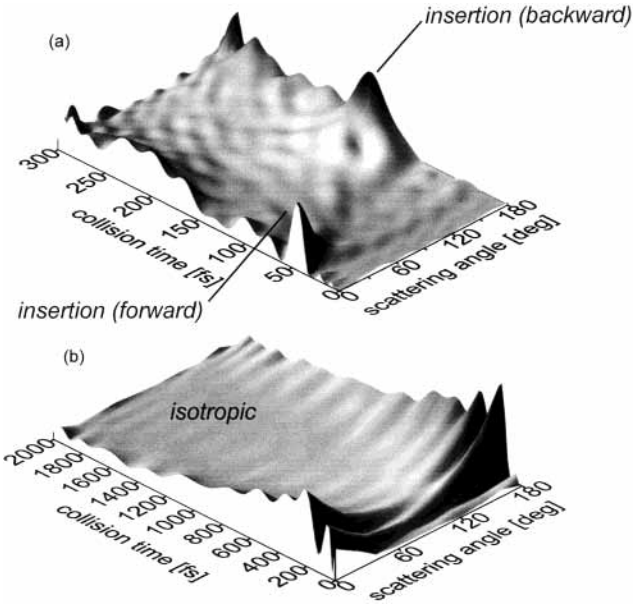

Figure 19. Three-dimensional plot of the combined distribution of classical collision times and scattering angles for the S(^{1}D) + H_2 ($v = 0$, $j = 0$) reaction at $E_c = 2.24$ kcal/mol. Top: collision times in the range $0 \le \tau_c \le 300$ fs. Bottom: collision times in the range $0 \le \tau_c \le 2000$ fs.

$\tau_t - \tau_i - \tau_f$, where τ_t is the total time of the trajectory and τ_i and τ_f are the initial and final times, respectively, where the strong interaction starts in the reagents and ends in the products. The values of τ_i and τ_f are determined by defining previously a distance parameter for reagents and products, ρ_r and ρ_p, respectively, by plotting a significant number of trajectories to determine the point where the strong interaction starts and ends. In the present case, values of $\rho_r = \rho_p = 2.5$Å have been employed.

Figure 18 shows the distribution of collision times for the S(^{1}D) + H_2 ($v = 0$, $j = 0$) reaction calculated at the collision energy of 2.24 kcal/mol. As can be seen, the distribution, which is quite smooth, peaks at collision times of ~300 fs and extends to collision times as long as 5 ps. It is worth noticing that the collision times obtained for the related O(^{1}D) + H_2 reaction at a similar collision energy[32] are significantly shorter that those obtained for the title reaction. Given the smaller depth of the H_2S well in comparison with that of H_2O, the longer lifetime of the H_2S collision complex has to be associated with the smaller exoergicity of the S(^{1}D) + H_2 reaction in comparison with O(^{1}D) + H_2. Thus, we can conclude that the S(^{1}D) + H_2 reaction is more statistical than the O(^{1}D) + H_2 system.

The present analysis shows no evidence of direct abstraction trajectories. All trajectories, even those with collision times smaller than 300 fs, go through an insertion mechanism. Figure 19 depicts a 3D representation of the combined distribution of collision times and scattering angles for the S(^{1}D) + H_2 ($v = 0$, $j = 0$) at 2.24 kcal/mol collision energy. The top panel corresponds to collision times smaller than 300 fs. As can be seen, the distribution at the shortest collision times is not isotropic, showing narrow peaks first forward ($\tau_c \approx 50$ fs) and later backward ($\tau_c \approx 150$ fs). From $\tau_c > 200$ fs up to the largest collision times (see bottom panel of Figure 19), the distribution becomes isotropic. An animated angle-distance 3D plot as a function of the collision time would show how the scattering appears first in forward, moving rapidly to backward and finally, for times longer than 200 fs, becoming isotropic. Thus, even for a prototypical statistical reaction characterized by a symmetric backward−forward DCS as the present one, the short-time dynamics involves a series of rich features as those shown in Figure 19.

IV. Conclusions

A detailed QM and QCT study of the S(^{1}D) + H_2 reaction has been presented. The theoretical results include reaction probabilities as a function of collision energy and integral and differential cross sections at two collision energies. In the QCT calculations, a GB procedure has been implemented for the assignment of product quantum states. A very good agreement

between both QM and QCT-GB theoretical methods has been found for state-to-state integral and differential cross sections. In particular, it is demonstrated in this work that, in order to get reliable QCT results when compared with the QM ones, the GB procedure must be followed for the assignment of product quantum states. The theoretical results have been employed to simulate the available experimental data in the form of angular distributions and product translational energy distributions. A general good agreement has been found between experiment and theory at 2.24 kcal/mol collision energy, whereas the agreement gets worse at the higher 3.96 kcal/mol collision energy. An analysis in terms of the classical collision times shows that the title reaction is more statistical than the $O(^1D) + H_2$ despite having a smaller depth of the well in the potential energy surface.

Acknowledgment. We are indebted to Kopin Liu for providing us with the experimental data. This work has been financed by the Spanish Ministry of Science and Technology (Project BQU2002-04627-C02-02) and by the European Commission within the RT Network *Reaction Dynamics* (Contract No. HPRN-CT-1999-00007). The QM dynamical calculations were performed on a NEC-SX5 vector supercomputer, through a grant from the "Institut du Développement des Ressources en Informatique Scientifique" in Orsay (France).

References and Notes

(1) Casavecchia, P. *Rep. Prog. Phys.* **2000**, *63*, 355.
(2) Liu, K. *Int. Rev. Phys. Chem.* **2001**, *20*, 189.
(3) Althorpe, S. C.; Clary, D. C. *Annu. Rev. Chem.* **2003**, *54*, 493.
(4) Liu, X.; Lin, J. J.; Harich, S.; Schatz, G. C.; Yang, X. *Science* **2000**, *289*, 1536.
(5) Aoiz, F. J.; Bañares, L.; Castillo, J. F.; Brouard, M.; Denzer, W.; Vallance, C.; Honvault, P.; Launay, J.-M. *Phys. Rev. Lett.* **2001**, *86*, 1729.
(6) Liu, X.; Lin, J. J.; Harich, S.; Yang, X. *Phys. Rev. Lett.* **2001**, *86*, 408.
(7) Aoiz, F. J.; Bañares, L.; Castillo, J. F.; Herrero, V. J.; Martínez-Haya, B.; Honvault, P.; Launay, J. M.; Liu, X.; Lin, J. J.; Harich, S. A.; Wang, C. C.; Yang, X. *J. Chem. Phys.* **2002**, *116*, 10692.
(8) Aoiz, F. J.; Bañares, L.; Castillo, J. F.; Herrero, V. J.; Martínez-Haya, B. *Phys. Chem. Chem. Phys.* **2002**, *4*, 4379.
(9) Rackham, E. J.; Huarte-Larranaga, F.; Manolopoulos, D. E. *Chem. Phys. Lett.* **2001**, *343*, 356.
(10) Balucani, N.; Cartechini, L.; Capozza, G.; Segoloni, E.; Casavecchia, P.; Volpi, G. G.; Aoiz, F. J.; Bañares, L.; Honvault, P.; Launay, J. M. *Phys. Rev. Lett.* **2002**, *89*, 013201−1.
(11) Bergeat, A.; Cartechini, L.; Balucani, N.; Capozza, G.; Phillips, L. F.; Casavecchia, P.; Volpi, G. G.; Bonnet, L.; Rayez, J.-C. *Chem. Phys. Lett.* **2000**, *327*, 197.
(12) Bañares, L.; Aoiz, F. J.; Honvault, P.; Bussery-Honvault, B.; Launay, J.-M. *J. Chem. Phys.* **2003**, *118*, 565.
(13) Zyubin, A. S.; Mebel, A. M.; Chao, S. D.; Skodje, R. T. *J. Chem. Phys.* **2001**, *114*, 320.
(14) Lee, S.-H.; Liu, K. *Appl. Phys. B* **2000**, *71*, 627.
(15) Lee, S.-H.; Liu, K. *J. Phys. Chem. A*, **1998**, *102*, 8637.
(16) Lee, S.-H.; Liu, K. *Chem. Phys. Lett.* **1998**, *290*, 323.
(17) Chao, S. D.; Skodje, R. T. *J. Phys. Chem.* **2001**, *105*, 2474.
(18) Ho, T.-S.; Hollebeek, T.; Rabitz, H.; Chao, S. D.; Skodje, R. T.; Zyubin, A. S.; Mebel, A. M. *J. Chem. Phys.* **2002**, *116*, 4124.
(19) Honvault, P.; Launay, J.-M. *Chem. Phys. Lett.* **2003**, *370*, 371.
(20) (a) Launay, J. M.; Le Dourneuf, M. *Chem. Phys. Lett.* **1989**, *163*, 178. (b) Launay, J. M.; Le Dourneuf, M. *Chem. Phys. Lett.* **1990**, *169*, 473.
(21) Launay, J. M. *Theor. Chim. Acta* **1991**, *79*, 183.
(22) Honvault, P.; Launay, J. M. *Chem. Phys. Lett.* **1998**, *287*, 270.
(23) Martínez-Haya, B.; Aoiz, F. J.; Bañares, L.; Honvault, P.; Launay, J. M. *Phys. Chem. Chem. Phys.* **1999**, *1*, 3415.
(24) Honvault, P.; Launay, J.-M. *J. Chem. Phys.* **2001**, *114*, 1057.
(25) Honvault, P.; Launay, J.-M. *J. Chem. Phys.* **1999**, *111*, 6665.
(26) Manolopoulos, D. E. *J. Chem. Phys.* **1986**, *85*, 6425.
(27) Aoiz, F. J.; Bañares, L.; Herrero, V. J. *J. Chem. Soc., Faraday Trans.* **1998**, *94*, 2483.
(28) Bonnet, L.; Rayez, J. C. *Chem. Phys. Lett.* **1997**, *277*, 183.
(29) Aoiz, F. J.; Bañares, L.; Herrero, V. J. *Chem. Phys. Lett.* **1999**, *310*, 277.
(30) Aoiz, F. J.; Bañares, L.; Brouard, M.; Castillo, J. F.; Herrero, V. J. *J. Chem. Phys.* **2000**, *113*, 5339.
(31) Pomerantz, A. E.; Ausfelder, F.; Zare, R. N.; Althorpe, S. C.; Aoiz, F. J.; Bañares, L.; Castillo, J. F. *J. Chem. Phys.* In press.
(32) Bañares, L. et al. Work in progress.